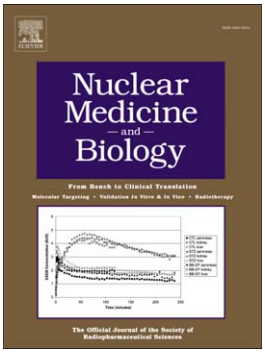

DOTA-Tetrazine Probes with Modified Linkers for Tumor Pretargeting

Tilman Läppchen, Raffaella Rossin, Tiemen R. van Mourik, Guillaume Gruntz, Freek J.M. Hoeben, Ron M. Versteegen, Henk M. Janssen, Johan Lub, Marc S. Robillard

PII: S0969-8051(17)30188-9
DOI: doi: 10.1016/j.nucmedbio.2017.09.001
Reference: NMB 7964

To appear in: *Nuclear Medicine and Biology*

Received date: 23 June 2017
Revised date: 31 August 2017
Accepted date: 5 September 2017

Please cite this article as: Läppchen Tilman, Rossin Raffaella, van Mourik Tiemen R., Gruntz Guillaume, Hoeben Freek J.M., Versteegen Ron M., Janssen Henk M., Lub Johan, Robillard Marc S., DOTA-Tetrazine Probes with Modified Linkers for Tumor Pretargeting, *Nuclear Medicine and Biology* (2017), doi: 10.1016/j.nucmedbio.2017.09.001

DOTA-Tetrazine Probes with Modified Linkers for Tumor Pretargeting

Abbreviated Title: DOTA-Tetrazine Probes for Tumor Pretargeting

Tilman Läppchen[1,2,3], Raffaella Rossin[1,5], Tiemen R. van Mourik[1], Guillaume Gruntz[1], Freek J.M. Hoeben[4], Ron M. Versteegen[4], Henk M. Janssen[4], Johan Lub[1], Marc S. Robillard[1,5*]

[1] Philips Research, High Tech Campus 11, 5656 AE Eindhoven, The Netherlands; [2] Department of Nuclear Medicine, Medical Center – University of Freiburg, Faculty of Medicine, University of Freiburg, Germany; [3] Department of Nuclear Medicine, Inselspital, Bern University Hospital and University of Bern, Bern, Switzerland; [4] SyMO-Chem BV, Den Dolech 2, 5612 AZ Eindhoven, The Netherlands; [5] Tagworks Pharmaceuticals BV, c/o Department of Nuclear Medicine and Radiology, Radboud University Medical Center, 6500 HB Nijmegen, The Netherlands

* Corresponding Author. Tel.: +31 6 25021525

E-mail address: marc.robillard@tagworkspharma.com (M. Robillard)

Keywords: Diels-Alder, tetrazine, trans-cyclooctene, pretargeting, antibodies, ^{177}Lu

Abstract

Introduction: Pretargeted radioimmunoimaging and -therapy approaches building on the bioorthogonal inverse-electron-demand Diels-Alder (IEDDA) reaction between strained *trans*-cyclooctenes (TCO) and electron-deficient tetrazines (Tz) have yielded impressive results in recent years and have proven a vital alternative to biological pretargeting systems. After improvement of the TCO-antibody conjugates, we here report on our evaluation of a new series of radiolabeled Tz-probes.

Methods: Four new Tz-probes were synthesized, radiolabeled with lutetium-177, and characterized *in vitro* in terms of lipophilicity, reactivity, and stability in PBS and mouse serum. The *in vivo* biodistribution profile and tumor-targeting potential of the probes was evaluated in LS174T tumor-bearing mice pretargeted with TCO-antibody conjugates using non-pretargeted mice as control.

Results: Radiolabeling of all probes proceeded in high yields providing the ^{177}Lu-labeled tetrazines in >95% radiochemical purity without any further purification. In mouse serum, half-lives of the probes varied between 8 and 13 h, with the exception of the most lipophilic probe, [^{177}Lu]**1b**, with a serum half-life of less than 1 h. This probe also showed the fastest blood clearance ($t_{1/2}$ = 5.4 min), more than 2-fold faster than PEG-linked probes [^{177}Lu]**3** and [^{177}Lu]**4**, and even 3-fold faster than the other small probes without the PEG-linker, [^{177}Lu]**1a** and [^{177}Lu]**2**. In the pretargeting experiments, tumor uptake of the lead probe [^{177}Lu]**4** (~6 %ID/g) was most closely approached by [^{177}Lu]**2**, followed by [^{177}Lu]**3** and [^{177}Lu]**1a**. While all the smaller and more lipophilic probes suffered from increased liver uptake, the PEG-linked probe [^{177}Lu]**3** with its additional negative charge surprisingly showed the highest kidney uptake among all of the probes.

Conclusion: The *in vitro* performance of some of the new tetrazine probes turned out to be comparable to the established lead probe [^{177}Lu]Lu-DOTA-PEG$_{11}$-Tz ([^{177}Lu]**4**). However, tumor pretargeting studies *in vivo* showed lower tumor uptake and increased uptake in non-target organs.

1. Introduction

After FDA approval of the first agents ibritumomab tiuxetan (Zevalin) and iodine tositumomab (Bexxar) more than a decade ago, radioimmunotherapy (RIT) is well established as a second-line therapy for treatment of refractory non-Hodgkins lymphoma [1]. One of the major limitations of conventional RIT with radiolabeled monoclonal antibodies (mAbs) is the high radiation dose to non-target tissues resulting from the combination of prolonged blood clearance and slow target uptake (reviewed in [2]). Pretargeted radioimmunotherapy (PRIT) addresses this issue by combining the superior targeting properties of antibodies with the favorable pharmacokinetics of smaller molecules (reviewed in [3, 4]). The method relies on tumor pretargeting with engineered mAbs having both affinity for a tumor-associated antigen and the capability to bind to a radioligand. The fast-clearing radioligand is then injected in a second step, after allowing sufficient time for accumulation of the mAbs in the tumor and clearance from blood. Currently, two pretargeting approaches have been clinically validated: bispecific antibodies with affinity for both the tumor and the radiolabeled small hapten [5], and antibody-conjugates making use of the streptavidin-biotin interaction [6]. While the first system requires extensive reengineering and perturbation of the parent mAb, streptavidin-biotin systems frequently suffer from immunogenicity, thereby precluding repeated treatment cycles [7]. Recently developed chemical pretargeting strategies relying on antibody modification with small tags may hold the potential to circumvent these issues (reviewed in [8, 9]). Among several bioorthogonal chemical reactions evaluated for this purpose, the inverse-electron-demand Diels-Alder (IEDDA) reaction between strained *trans*-cyclooctenes (TCO) and electron-deficient tetrazines (Tz) has yielded promising results for pretargeted radioimmunoimaging and –therapy in preclinical studies [10-19], whereas the Staudinger ligation and the strain-promoted alkyne-azide cycloaddition reaction (SPAAC) suffered from a number of limitations [20-22]. Following our initial report on pretargeted tumor imaging in live mice using a TCO-antibody conjugate and an ^{111}In-labeled Tz-probe (Fig. 1) [10], we and others have continuously improved the system by developing more reactive TCO-tags

with increased *in vivo* stability [14] and dedicated Tz-probes for radiolabeling with copper-64 [12], gallium-68 [23], fluorine-18 [17, 24], carbon-11 [25, 26], technetium-99m [27], and iodine-125 [28]. In the meantime, Tz-probes with reduced gastrointestinal clearance have shown promise for pretargeted immuno-PET of colorectal cancer [16, 18] and radioimmunotherapy of pancreatic ductal adenocarcinoma [19] in preclinical studies. To further increase tumor-to-blood ratios and maximize tumor dose in pretargeted radioimmunotherapy, we have introduced a rapid bioorthogonal chemical clearing approach for removal of residual circulating TCO-conjugated antibodies from blood prior to injection of the radiolabeled probe [13]. Finally, our efforts resulted in an optimized pretargeting protocol employing antibody constructs with a more reactive and less hydrophobic TCO-tag with higher *in vivo* stability, and improved tumor accumulation [15].

Having optimized the reactivity and pharmacokinetics of the TCO-tagged antibody, in this work, we set out to explore the parameters that govern *in vivo* performance of the tetrazine probe, which may in the future enable the design of a probe with improved tumor uptake and reduced uptake in the kidney, the organ retaining most of the activity apart from the tumor [13]. Inspired by earlier investigations suggesting that an increase of negative charges in DOTA- and DTPA-conjugated peptides resulted in reduction of renal uptake [29, 30], we designed a Tz-probe **3** (Fig. 2), in which the Tz-moiety is attached via a PEG_{10}-thioureabenzyl-linker to the carbon backbone of the DOTA, allowing for as many as four carboxymethyl functionalities and resulting in a net negative charge of the ^{177}Lu-labeled probe at physiologic pH. Aiming at probes with better tumor penetration and a more homogenous uptake, we created the shorter Tz-DOTA derivatives **1a** and **1b** linked by straight chain C_6- and C_{11}-amidoalkyl groups, respectively, and probe **2**, which in fact corresponds to the original probe **4** without the PEG-spacer (Fig. 2). The new probes were evaluated *in vitro* and *in vivo* employing our previously developed clearing agent strategy [13] and pretargeting components (Fig. 2), and benchmarked against lead probe **4**.

2. Experimental

2.1. Chemistry

Synthetic procedures and spectral data for the new Tz-probes **1a/b**, **2**, **3**, and **4** are described in §1 and §2 of the Supplemental Information associated with this article. Preparation of CC49-TCO (**6**) and galactose-albumin-tetrazine (**5**) has been reported elsewhere [10, 13].

2.2. Radiochemistry

Radioiodination of CC49-TCO (**6**) was performed with the Bolton-Hunter method, followed by purification and quality control according to a published procedure [13]. A detailed procedure including results is also reported in § 3.1 of the Supplemental Information. For animal experiments, the specific activity of the [^{125}I]I-CC49-TCO was adjusted to 2–5 kBq/μg by adding nonradioactive CC49-TCO.

The DOTA-conjugated Tz-probes **1a/b**, **2**, **3**, and **4** were dissolved in 0.2 M ammonium acetate pH 7.0 at concentrations of 1-2 mg/mL and stored at –80°C before use. Radiolabeling for the *in vitro* stability studies was performed by combining suitable volumes of probe stock solutions (corresponding to 10 μg for tetrazine **1a/b** and **2**, 15 μg for tetrazine **3** and **4**) with [^{177}Lu]$LuCl_3$ (20 – 35 MBq; Perkin-Elmer) in 0.2 M ammonium acetate pH 5.5 (total volume of the reaction mixture was 20 μL) and incubating at 60°C for 5 min in a thermomixer (350 rpm). Following addition of 5 μL of 10 mM diethylenetriaminepentaacetic acid (DTPA) and incubation for another 5 min at 60°C, radiochemical yield and purity were assessed by radio-iTLC and radio-HPLC, respectively. Molar activities (A_m) for the ^{177}Lu-labeled Tz-probes **1a**, **1b**, **2**, **3**, and **4** were 2.28 ± 0.21, 2.54 ± 0.65, 2.02 ± 0.42, 2.85 ± 0.28, and 2.62 ± 0.40 MBq/nmol, respectively (n = 6 for each probe). For investigation of the *in vitro* reaction kinetics, labeling was performed according to the same procedure, but at higher specific activity (50 – 60 MBq [^{177}Lu]$LuCl_3$, 5 μg tetrazine, i.e., A_s ~ 10 – 12 MBq/μg), and

gentisic acid (20 µL of a 20 mg/mL solution in 0.9% saline - 1.0 M Na_2CO_3, 9:1) was added post-labeling to prevent autoradiolysis.

For the *in vivo* studies, the tetrazines were labeled to a molar activity (A_m) of 0.11 – 0.15 MBq/nmol by combining a suitable volume of the Tz-stock solutions with [^{177}Lu]$LuCl_3$ in 1.0 M NH_4OAc pH 5.0 (10 µL) and incubating at 60°C for 5 min, followed by addition of gentisic acid (50 µL of a 20 mg/mL solution in 0.9% saline - 1.0 M Na_2CO_3, 9:1) and 10 mM DTPA (5 µL). After incubation at 60°C for another 5 min, aliquots of the labeling mixture were analyzed by radio-TLC and radio-HPLC, and the reaction mixture diluted with sterile 0.9% saline for animal experiments, each dose (80 µL, ca. 1 MBq) containing 6.67 nmol of tetrazine and 100 µg of gentisic acid.

2.3. In vitro characterization of radiotracers

2.3.1. Distribution coefficient Log$D_{7.4}$ in 1-octanol / PBS pH 7.4

Log$D_{7.4}$ values were measured using the shake flask method. Tetrazines were radiolabeled according to the protocol for the *in vitro* studies, however, apart from [^{177}Lu]$LuCl_3$, also non-radioactive $LuCl_3$ (0.8 eq. with respect to probe) was added to the labeling mixture. The labeled tetrazines were additionally purified by passing through a C_8 Sep-Pak® cartridge and eluting with ethanol, mainly to remove traces of highly polar [^{177}Lu]LuDTPA. To 1-octanol (0.5 mL) and PBS pH 7.4 (0.5 mL), which had been pre-saturated with each other, was added 5 µL of the purified ethanolic radiotracer stock solution (about 1 MBq, radiochemical purity >95%, radio-HPLC), and the phases were thoroughly mixed using a vortex (3 × 30 sec) then incubated at room temperature in a thermomixer (550 rpm) for 5 min. This procedure was repeated twice to establish a stable equilibrium between the phases. Following phase separation by centrifugation in an eppendorf centrifuge at 16,100 × g for 5 min, aliquots of both phases (3 × 25 µL for the aqueous phase, 3 × 100 µL for the organic phase) were counted in a γ-counter (Wizard 1480; Perkin Elmer). Log$D_{7.4}$ was calculated as log [(cpm in octanol) / (4 × cpm in PBS)]. For each probe, all determinations were performed in triplicate.

2.3.2. Radiotracer stability in PBS pH 7.4 and in mouse serum

The ^{177}Lu-labeled Tz-probes **1a/b**, **2**, **3**, and **4** were incubated at 37°C under gentle agitation (350 rpm) in either PBS pH 7.4 or 50% mouse serum/PBS (Balb/C mouse serum, purchased from Innovative Research, and filtered through a 0.45 µm PTFE syringe filter before use) at a concentration of 4.8 nmol/mL (corresponding to the concentration in blood achieved after *i.v.* injection of the probes in the animal experiments) and activity concentrations of 10 – 15 MBq/mL. For the PBS-incubation, aliquots were directly analyzed by radio-HPLC immediately after addition and mixing, and after 0.5, 1, 2, 4, and 20 h. For the serum samples, 100 µL aliquots were retrieved at the same time points, thoroughly mixed with an equal volume of ice-cold acetonitrile, and proteins separated by centrifugation (16,100 × g, 5 min). An aliquot of the supernatant was removed for radio-HPLC, and another aliquot (50 µL) for measuring of radioactivity in the supernatant. The remaining supernatant was discarded, and radioactivity of the pellet and supernatant-aliquot determined in a γ-counter for quantification of probe binding to serum proteins. To eliminate any effects due to sample processing, stability values (% intact radiotracer) were reported relative to the control sample (t = 0), for which the amount of intact probe was set to 100%. All determinations (for each probe and each time point) were performed in triplicate. Serum stability half-lives were calculated from a one-phase exponential decay fit of the data.

2.3.3. Reaction kinetics between CC49-TCO and ^{177}Lu-labeled Tz-probes

The Tz-probes **1a/b**, **2**, **3**, and **4** were radiolabeled at high specific activity (10 MBq/µg) as described above. Directly before the experiment, a weighted aliquot of a CC49-TCO **6** stock solution (8.8 TCO/mAb) was diluted with pre-warmed (37°C) 50% mouse serum / PBS pH 7.4 (filtered Balb/C mouse serum) to yield a final mAb-concentration of 10 µg/mL in a volume of about 1 mL (corresponding to a TCO-concentration of 587 nM). The reaction was started by addition of the ^{177}Lu-labeled Tz (several µL of a 10 – 20 fold diluted radiolabeling mixture) to give a final

concentration of 29 nM (1/20th of TCO-concentration) in the reaction mixture. After thorough mixing, 20 μL samples of the reaction mixture were withdrawn at selected times (15, 30, 45, 60, 120, and 300 sec) and quenched with an excess of non-radioactive tetrazine. Aliquots of each reaction mixture were analyzed by SDS-PAGE and phosphor imager and the cycloaddition yields were calculated from the radioactivity in the bands corresponding to the unreacted and mAb-bound ^{177}Lu-labeled tetrazine (Supplemental Information, § 3.3, Figure S6 and S7). The pseudo first-order rate constants (k_{obs}) were determined from the fits to a first-order exponential.

2.4. Animal studies

Mice were housed and handled according to institutional guidelines complying with European legislation and the Dutch national law "Wet op de Dierproeven" (Staatsblad 1985, 336). Approval of the animal welfare committee of Maastricht University (the Netherlands) was obtained prior to the commencement of the studies. Animals were kept in a temperature-controlled environment with a 12-hour light/12-hour dark cycle. They received a standard diet (Sniff R/M-H, Sniff Spezialdiäten GmbH, Soest, The Netherlands) and acidified water *ad libitum*. The human colon cancer cell line LS174T was obtained from ATCC and maintained in Eagle's minimal essential medium (Sigma) supplemented with 10% heat inactivated fetal calf-serum (Gibco), penicillin (100 U/mL), streptomycin (100 μg/mL) and 2 mM Glutamax. Female nude Balb/C mice (18 – 23 g body weight; Charles River Laboratories) were inoculated subcutaneously with 5 × 10^6 LS174T cells in 100 μL of sterile PBS, and were used when the tumors had reached a size of 70–250 mm^3 (typically after 7–10 days). Tumor weights at the time of biodistribution were 0.28 ± 0.11 g (mean ± SD). Sample radioactivity was measured in a γ-counter (Wizard 1480, Perkin Elmer) using either a single-isotope protocol with an energy window of 10–380 keV for lutetium-177, or a dual-isotope protocol with energy windows of 10–80 keV and 155–380 keV for iodine-125 and lutetium-177, respectively, with cross contamination correction. Radioactivity of the biodistribution samples was counted along with

standards to determine the percentage of injected dose (%ID) per gram of tissue and per organ. The %ID/organ values for stomach, small and large intestines relate to organ including content.

2.4.1. Dual-isotope biodistribution experiments in pretargeted mice

Four groups of tumor-bearing mice (n = 3–4) were intravenously injected with ^{125}I-labeled CC49-TCO (**6**) (average of 7 TCOs/mAb; 100 μg in 100 μL of saline per mouse; 0.20–0.45 MBq), followed by two doses of clearing agent (**5**) (160 μg in 100 μL of saline per dose) after 30 h and 48 h. Two hours after the last clearing agent injection, each group of mice was injected with one of the different ^{177}Lu-labeled Tz-probes **1a/b**, **2**, **3**, and **4** (per dose: 6.7 nmol tetrazine in 80 μL of saline containing 100 μg of gentisic acid; 0.6–1.0 MBq). Mice were euthanized 3 hours after [^{177}Lu]Lu-tetrazine injection, blood was withdrawn, tissues and organs of interest were collected, blotted dry, weighted, combined with 1 mL of PBS, and counted in a γ-counter (dual-isotope protocol).

2.4.2. Tetrazine blood clearance and biodistribution in non-pretargeted tumor-bearing mice

Each of four groups of tumor-bearing mice (n = 3–4) was intravenously injected with one of the different ^{177}Lu-labeled Tz-probes **1a/b**, **2**, **3**, and **4** (per dose: 6.7 nmol tetrazine in 80 μL of saline containing 100 μg of gentisic acid; 0.6–1.0 MBq). Mice were serially bled at selected time points (2, 5, 10, 20, 40, and 60 min post probe injection; ca. 20 μL per time point), and euthanized 3 hours after [^{177}Lu]Lu-Tz injection. Blood was withdrawn, tissues and organs of interest were collected, and radioactivity was measured in a γ-counter (single-isotope protocol).

2.5. Data analysis

Unless stated otherwise, all data are reported as mean ± standard deviation (SD). Curve fitting and calculation of rate constants, half-lives, and two-tailed unpaired t tests were performed with GraphPad Prism version 6.05.

3. Results and discussion

3.1. Synthesis of tetrazine probes and radiolabeling

Tetrazine-*n*-alkyl-DOTA probes **1a** and **1b** were assembled from 2-cyanopyridine, hydrazine and *N*-Boc-protected 2-cyano-5-amidoalkylaminopyridines **7a** and **7b**, which had been obtained in two steps from the corresponding straight-chain alkylaminocarboxylic acids and 2-cyano-5-aminopyridine (Fig. 3). After oxidation with sodium nitrite, Boc-deprotection with TFA, and coupling to DOTA-mono-(*N*-hydroxysuccinimide)-ester, the target compounds were obtained in overall yields of 25% and 14%, respectively. Compound **2**, a shorter version of lead compound **4** without the PEG-spacer, was prepared from tetrazine **11** by coupling with 2-aminoethyl-mono-amide-DOTA-tris-*t*Bu-ester **12** followed by *t*Bu-deprotection with TFA (Fig. 3, bottom left). The PEG_{10}-thioureabenzyl-linked compound **3** with four carboxymethyl functionalities, finally, was readily accessible from tetrazine **14**, a common precursor in the synthesis of lead compound **4**, which after Boc-deprotection is coupled to 2-(p-isothiocyanatobenzyl)-DOTA **15** (Fig. 3, bottom right). The HPLC-purified probes were conveniently radiolabeled with lutetium-177 at 60ºC in minutes with radiochemical yields typically exceeding 98%. Radiochemical purity after DTPA challenge was always >95%, allowing direct use of the labeling mixtures for the *in vivo* and *in vitro* studies without any further purification.

3.2. Probe evaluation in vitro

The physicochemical properties of the Tz-probes are summarized in Table 1, together with their *in vitro* stability data in PBS and 50% mouse serum/PBS, and their reactivity towards the TCO-tagged antibody CC49 **6**, expressed as pseudo first-order rate constants k_{obs}. In addition, HPLC metabolite profiles and comprehensive stability data for all time points (0.5, 1, 2, 4 h, and 20 h) are provided in the Supplemental Tables S1, S2, and S3.

The hydrophilic PEG-linked probes [^{177}Lu]**3** and [^{177}Lu]**4** display very similar profiles with stability half-lives at 37ºC of about 25 h in PBS and 8 h in 50% mouse serum. Both probes were primarily degraded to slightly more polar metabolites eluting about 1 – 2 min before the parent probe on radio-HPLC. Interestingly, HPLC-retention time (R_t) of the main metabolite after incubation in 50% serum was different (about 1 min shorter) than retention time of the main metabolite after incubation in PBS, suggesting different species are formed in these media (Supplemental Information, § 3.2, Tables S1 and S2, and Figures S4 and S5). Furthermore, incubation in PBS resulted in a higher level of highly hydrophilic metabolites (R_t ~ 2 – 2.5 min), presumably arising from cleavage of the [^{177}Lu]LuDOTA group. Nevertheless, even after incubation in PBS, these highly hydrophilic species generally account for less than 20% of the total metabolites, while the remaining >80% are consisting of the main metabolites mentioned above. The smaller and slightly less hydrophilic probes [^{177}Lu]**1a** and [^{177}Lu]**2** turned out to be more stable, particularly in 50% mouse serum ([^{177}Lu]**1a**: $t_{1/2}$ = 11.3 h; [^{177}Lu]**2**: $t_{1/2}$ = 13.4 h). Different from the PEG-linked probes [^{177}Lu]**3** and [^{177}Lu]**4**, however, serum incubation of [^{177}Lu]**1a** and [^{177}Lu]**2** mainly yielded the highly polar metabolite eluting with R_t = 2.5 min on radio-HPLC (accounting for >80% of total metabolites). Probe [^{177}Lu]**1b**, finally, a close analog of [^{177}Lu]**1a** with double length of the alkyl linker and substantially increased lipophilicity, proved to be the least stable of all probes, with a half-life in 50% serum/PBS of less than one hour and clean degradation into a single slightly more polar metabolite (HPLC, R_t = 10.6 min). All probes only showed a low degree of serum protein binding (Supplemental Table S2) ranging from 5.6 ± 1.2% (n = 3, 30 min incubation time) for lead probe [^{177}Lu]**4** to 10.4 ± 3.4% (n = 3) for [^{177}Lu]**1b**, the most lipophilic probe in the series.

Apart from probe stability, also the relative reactivity of the ^{177}Lu-labeled Tz-probes towards the mAb-bound TCOs and the Tz-pharmacokinetics, particularly blood clearance, are important parameters impacting tumor uptake. Even though all probes contain the same bis-(2-pyridyl)-1,2,4,5-tetrazine group, we have nevertheless determined the relative reaction rates of the Tz-probes (Table

1), and have found differences in reactivity. [^{177}Lu]**1b**, the least stable probe with the fastest blood clearance, turned out to be the most reactive, followed by [^{177}Lu]**1a**, its more hydrophilic analog with shorter alkyl-linker. The remaining probes, [^{177}Lu]**2** and [^{177}Lu]**3**, showed pseudo first-order rate constants (k_{obs}) similar to the lead probe [^{177}Lu]**4**. Importantly, "enforced hydrophobic interactions" have been suggested to provide an additional driving force for the IEDDA reaction due to reduction of the solvent-exposed hydrophobic surface area of the reactants in aqueous media [31, 32]. Along this line, increasing lipophilicity of the IEDDA reaction partners may result in higher reaction rates, and it is not surprising that the most hydrophobic ^{177}Lu-labeled Tz-probes in the series, [^{177}Lu]**1a** and [^{177}Lu]**1b** in particular, indeed displayed the highest k_{obs} in serum.

3.3. Comparative in vivo study: Tumor uptake, biodistribution, and blood clearance

The new Tz-probes were evaluated *in vivo* and benchmarked against lead probe **4** employing our previously established pretargeting protocol based on the TAG-72 targeting mAb CC49 conjugated to axially substituted TCO tags via oxymethylbenzamide linkages (CC49-TCO **6**, Fig. 2) [14] and a bioorthogonal clearing agent strategy [13]. Briefly, CC49-TCO **6** was radiolabeled with iodine-125 via the Bolton-Hunter method (isolated radiochemical yield after purification 22.4 ± 7.3%, n = 5, radiochemical purity >99%, detailed data in Supplemental Information, § 3.1), and intravenously administered to LS174T tumor-bearing mice (n = 3–4 per group), followed by two doses of clearing agent **5**, 30 and 48 h post mAb injection, and finally the ^{177}Lu-labeled tetrazines two hours after the last clearing agent injection. Dual-isotope biodistribution data 3 h post tetrazine injection are summarized in Table 2.

For comparison, control experiments were performed in non-pretargeted LS174T tumor-bearing mice (n = 3–4 per group), which only received ^{177}Lu-labeled tetrazines and were sacrificed 3 h post injection. Selected biodistribution data from these experiments are reported in Table 3. In addition, blood-clearance half-lives (Table 1 and Supplemental Table S6) were calculated from one-phase

exponential decay fits of blood radioactivity data from blood-sampling (Fig. 4). While [^{177}Lu]**3** displayed comparable blood kinetics to lead probe [^{177}Lu]**4**, the smaller probes [^{177}Lu]**1a** and [^{177}Lu]**2** were retained in blood for longer time periods ($t_{1/2} \approx 18$ min), and the most lipophilic probe [^{177}Lu]**1b** was eliminated from blood with a blood clearance half-life of 5.4 min, 2-fold faster than lead probe [^{177}Lu]**4** (Table 1). On a general note, all blood clearance data are based on total blood radioactivity and do not distinguish between the intact radiotracer and circulating metabolites (*vide infra*).

In the pretargeting experiments (Table 2), tumor uptake of the new Tz-probes varied considerably, but all of them showed lower uptake than lead probe [^{177}Lu]**4**. Tumor targeting of the lead probe was most closely approached by [^{177}Lu]**2**, a shorter version of this probe without the PEG-spacer. However, [^{177}Lu]**2** also displayed an almost 15-fold higher liver uptake, while at the same time not leading to significantly reduced uptake in the kidney. With a 2-atom shorter linker without the additional amide group, the structurally closely related probe [^{177}Lu]**1a** resulted in an almost 3-fold higher liver uptake compared to [^{177}Lu]**2** alongside with a 50% lower tumor uptake. Doubling the length of the alkyl-linker from a pentyl-group in [^{177}Lu]**1a** to a decyl-group in probe [^{177}Lu]**1b** led to a dramatic increase in liver uptake up to almost 14% ID/g and a concomitant decrease in tumor uptake down to only about 1% ID/g, which is presumably associated with the significantly shorter blood elimination half-life of this probe.

On a general note, as expected, increasing probe lipophilicity appears to correlate with a higher liver uptake, with the hydrophilic probes [^{177}Lu]**3** and [^{177}Lu]**4** (both around 0.2% ID/g) at the lower range, [^{177}Lu]**2** (2.63 ± 0.30 %ID/g) and [^{177}Lu]**1a** (6.73 ± 1.40 %ID/g) in the middle section, and the most lipophilic [^{177}Lu]**1b** (13.63 ± 1.06 %ID/g) at the upper range of the scale (Table 2), covering lipophilicity differences of 4 orders of magnitude (Table 1). The high uptake in the liver and intestines, together with an almost 5-fold lower kidney uptake than lead probe [^{177}Lu]**4**, suggest that [^{177}Lu]**1b** is predominantly cleared via the hepatobiliary route. In contrast, the probes of intermediate

lipophilicity, [^{177}Lu]**1a** and [^{177}Lu]**2**, show a kidney uptake similar to lead probe [^{177}Lu]**4**, pointing towards partial renal clearance of the probes alongside hepatobiliary excretion. Strikingly and in contrast to our expectations, the only negatively charged probe that we have studied, the PEG_{10}-thioureabenzyl-linked probe [^{177}Lu]**3**, displayed the highest kidney uptake within the series, more than 2-fold the uptake of lead probe [^{177}Lu]**4**.

Comparison of our findings with recently published data from ^{64}Cu-labeled probes based on the related 3-4-(benzylamine)-1,2,4,5-tetrazine instead of our bis(pyridino)-system revealed similar trends [16]. Comparable to [^{177}Lu]**1a** of the present work, the smallest probe in that study [16], a benzylamino-tetrazine moiety attached to a NOTA-chelator with a connecting C5-linker via amide bonds, is predominantly excreted via the gut with highest accumulation in the large intestines and its content and only low kidney uptake. Introduction of a PEG_7-linker led to a probe with increased renal clearance and accelerated intestinal excretion, which correlates well with our results obtained for the PEG_{10}-linked probes [^{177}Lu]**3** and **[**^{177}Lu]**4**.

Taken together, in the series [^{177}Lu]**1b** → [^{177}Lu]**1a** → [^{177}Lu]**2** of the smaller probes without PEG-spacer, the decrease in probe lipophilicity and liver uptake apparently translates into a higher tumor uptake. Indeed, despite its almost 2-fold higher reactivity compared to lead probe [^{177}Lu]**4**, the low tumor targeting potential of [^{177}Lu]**1b** is not surprising given its short circulation half-life ($t_{1/2}$ = 5.4 min) and low stability *in vitro* ($t_{1/2}$ in 50% serum < 1 h). For the other probes, however, there is no simple correlation between tumor uptake and reactivity, *in vitro* stability and *in vivo* blood clearance. In fact, [^{177}Lu]**1a** and [^{177}Lu]**2** were expected to demonstrate superior tumor targeting, since these probes show the slowest blood elimination *in vivo* ($t_{1/2} \approx 18$ min) the highest stability *in vitro* ($t_{1/2}$ in 50% serum >11 h), and a reactivity comparable or slightly superior to the lead probe [^{177}Lu]**4** (Table 1). Apparently, the prediction of the *in vivo* behavior of the probes from their *in vitro* properties is not straightforward. The discrepancy between the *in vivo* and *in vitro* behavior may be related to a different metabolism of the probes *in vivo*. This issue has been described for a number of

radiopharmaceuticals, in particular radiopeptides, and has recently received considerable attention [33]. *In vitro* serum/blood incubation studies usually tend to overestimate the actual stability [33-37]. Moreover, *in vivo* metabolism may give rise to additional, structurally different metabolites than those identified in serum incubation studies *in vitro* [34]. While some of these metabolites may be identified by *in vitro* incubation studies using tissue homogenates (typically from liver and kidney as the main metabolizing organs), a true assessment of radiotracer metabolism and stability can often only be obtained from *in vivo* studies, among others due to the involvement of ectoenzymes on epithelial cells on various organs and tissues in the body [33, 34, 38]. Importantly, the radiotracer blood elimination curves (Fig. 4) only convey very limited information, as they are based on the total blood radioactivity, without any distinction between the intact radiotracer and circulating metabolites. Depending on their type and structure, most of the different ^{177}Lu-labeled metabolites may not be reactive towards TCOs, resulting in a much lower probe bioavailability than suggested based on the non-metabolite-corrected radiotracer blood elimination curve. Unfortunately, in-depth investigation of probe bioavailability and characterization of metabolites requires a complete metabolism study, which is beyond the scope of this paper. Along these lines, it is not surprising that the slower blood clearance and higher *in vitro* stability of [^{177}Lu]**1a** and [^{177}Lu]**2** compared to lead probe [^{177}Lu]**4** is not necessarily leading to an improved *in vivo* performance.

Comparison of the biodistributions of the pretargeted and non-pretargeted mice (Table 2 versus Table 3) shows considerable agreement. Apart from [^{177}Lu]**1a**, statistically significant differences were only found in the liver, kidney, or lung (Table 3). Evidently, the clearing agent strategy has proven effective, since the remaining level of [^{125}I]I-CC49-TCO in the blood of pretargeted mice is too low to result in statistically significant differences between the blood values of the ^{177}Lu-labeled tetrazines in pretargeted mice and non-pretargeted mice. At the same time, non-specific tumor uptake in the non-pretargeted group of mice (Table 3) was significantly lower than tumor uptake in the

pretargeted group of mice, which is in good agreement with the high level of [^{125}I]I-CC49-TCO in the tumor (Table 2 and Supplemental Table S4).

The lower tumor uptake of the new probes, together with increased uptake in most non-target tissues, translates into lower tumor-to-organ ratios, as expected (Fig. 5). In fact, perusal of Table 2 indicates that organ uptake values for all probes are higher than or about equal to lead probe [^{177}Lu]**4**, the considerably lower kidney uptake of probe [^{177}Lu]**1b** being the sole exception. However, even in this case, the reduction in kidney uptake proves not sufficient to compensate for the substantially lower tumor uptake of [^{177}Lu]**1b** and still results in a lower tumor-to-kidney ratio compared to [^{177}Lu]**4**. Although all new probes show lower tumor-to-blood ratios than lead probe [^{177}Lu]**4**, the underlying reason is different; for [^{177}Lu]**1b** it is mainly caused by the lower tumor uptake, while for [^{177}Lu]**1a** and [^{177}Lu]**2**, it is mainly determined by the higher blood uptake. Since blood retention of [^{177}Lu]**1a** and [^{177}Lu]**2** is almost identical in the pretargeted and non-pretargeted groups of mice (Table 2 versus Table 3), the higher blood retention of these probes compared to [^{177}Lu]**4** is presumably not related to reaction with residual circulating [^{125}I]I-CC49-TCO, but is instead an intrinsic property of these probes and a result of slower blood clearance (Table 1) of the intact probes or their radioactive metabolites (*vide supra*). Indeed, the blood and tumor levels of [^{125}I]I-CC49-TCO in the experiments described here (0.46 ± 0.18 %ID/g and 20.71 ± 3.37 %ID/g, Table 2) show a rather low variation between the groups (see Supplemental Table S4 for detailed data per group) and are comparable to previously reported values (0.19 ± 0.04 %ID/g and 22.22 ± 2.58 %ID/g, n = 4) [15], further supporting the conclusion that the higher blood and lower tumor levels of the new ^{177}Lu-labeled tetrazines are mainly related to the probes and not to differences in the [^{125}I]I-CC49-TCO biodistribution. Along this line, normalization of ^{177}Lu-Tz tumor uptake to the individual [^{125}I]I-CC49-TCO uptake for each mouse led to almost identical values, but mostly smaller SD's (Supplemental Table S5).

4. Conclusion

We have prepared a new series of tetrazine probes for application in pretargeted radioimmunoimaging and –therapy based on the inverse-electron-demand Diels-Alder reaction between strained trans-cyclooctenes and electron-deficient tetrazines. Apart from [^{177}Lu]**1b** with an *in vitro* serum stability half-life of less than 1 h, all of the new tetrazine probes show similar or superior stability to lead probe [^{177}Lu]**4**. At the same time, [^{177}Lu]**1b** also turned out to be the most reactive probe *in vitro*, followed by its shorter C5-linker analogue [^{177}Lu]**1a**, and finally the other probes, which demonstrated a reactivity comparable to the lead probe. In contrast to their *in vitro* performance, the *in vivo* profile of the new probes in tumor pretargeting studies did not meet our expectations. All of the probes showed lower tumor uptake than lead probe [^{177}Lu]**4** and were characterized by higher uptake in non-target organs, resulting in consistently lower tumor-to-organ ratios. While the smaller, more lipophilic probes particularly suffered from higher liver uptake, the negatively charged PEG-linked probe [^{177}Lu]**3** surprisingly showed the highest kidney uptake. Notably, the longer blood clearance half-lives and the increased serum stability of the small probes [^{177}Lu]**1a** and [^{177}Lu]**2** (the best-performing probe beside the lead probe), did not translate into more effective tumor targeting. Further efforts towards the design of improved tetrazine probes should presumably focus on hydrophilic probes with significantly improved reactivity.

Acknowledgments

We thank Reece Kenny for support with the *in vitro* stability studies, Mariëlle van Egmond for assistance with chemical syntheses, and Jeroen van den Berg, Daniëlle Beelen, and Hugo Knobel for technical support with NMR- and LC-MS analyses. Dr. Iris Verel, Caren van Kammen, Carlijn van Helvert, and Monique Berben are gratefully acknowledged for assistance in planning and executing of the *in vivo* studies. Part of this work was funded by the Center for Translational Molecular

Medicine – Mammary Carcinoma Molecular Imaging for Diagnosis and Therapeutics (CTMM-MAMMOTH, grant 2010249, project 03O-201).

References

[1] Martinez A, Martinez-Ramirez M, Martinez-Caballero D, Beneit P, Clavel J, Figueroa G, et al. Radioimmunotherapy for non-Hodgkin's lymphoma; positioning, safety, and efficacy of 90Y-Ibritumomab. 10 years of experience and follow-up. Rev Esp Med Nucl Imagen Mol 2017;36:13-9.

[2] Larson SM, Carrasquillo JA, Cheung NK, and Press OW. Radioimmunotherapy of human tumours. Nat Rev Cancer 2015;15:347-60.

[3] Frampas E, Rousseau C, Bodet-Milin C, Barbet J, Chatal JF, and Kraeber-Bodere F. Improvement of radioimmunotherapy using pretargeting. Front Oncol 2013;3:159.

[4] van de Watering FC, Rijpkema M, Robillard M, Oyen WJ, and Boerman OC. Pretargeted imaging and radioimmunotherapy of cancer using antibodies and bioorthogonal chemistry. Front Med (Lausanne) 2014;1:44.

[5] Schoffelen R, Sharkey RM, Goldenberg DM, Franssen G, McBride WJ, Rossi EA, et al. Pretargeted immuno-positron emission tomography imaging of carcinoembryonic antigen-expressing tumors with a bispecific antibody and a 68Ga- and 18F-labeled hapten peptide in mice with human tumor xenografts. Mol Cancer Ther 2010;9:1019-27.

[6] Bailly C, Bodet-Milin C, Rousseau C, Faivre-Chauvet A, Kraeber-Bodere F, and Barbet J. Pretargeting for imaging and therapy in oncological nuclear medicine. EJNMMI Radiopharmacy and Chemistry 2017;2:6.

[7] Goldenberg DM, Chang CH, Sharkey RM, Rossi EA, Karacay H, McBride W, et al. Radioimmunotherapy: is avidin-biotin pretargeting the preferred choice among pretargeting methods? Eur J Nucl Med Mol Imaging 2003;30:777-80.

[8] Rossin R and Robillard MS. Pretargeted imaging using bioorthogonal chemistry in mice. Curr Opin Chem Biol 2014;21:161-9.

[9] Meyer JP, Adumeau P, Lewis JS, and Zeglis BM. Click Chemistry and Radiochemistry: The First 10 Years. Bioconjugate Chem 2016;27:2791-807.

[10] Rossin R, Verkerk PR, van den Bosch SM, Vulders RC, Verel I, Lub J, et al. In vivo chemistry for pretargeted tumor imaging in live mice. Angew Chem Int Ed Engl 2010;49:3375-8.

[11] Devaraj NK, Thurber GM, Keliher EJ, Marinelli B, and Weissleder R. Reactive polymer enables efficient in vivo bioorthogonal chemistry. Proc Natl Acad Sci USA 2012;109:4762-7.

[12] Zeglis BM, Sevak KK, Reiner T, Mohindra P, Carlin SD, Zanzonico P, et al. A pretargeted PET imaging strategy based on bioorthogonal Diels-Alder click chemistry. J Nucl Med 2013;54:1389-96.

[13] Rossin R, Läppchen T, van den Bosch SM, Laforest R, and Robillard MS. Diels-Alder reaction for tumor pretargeting: in vivo chemistry can boost tumor radiation dose compared with directly labeled antibody. J Nucl Med 2013;54:1989-95.

[14] Rossin R, van den Bosch SM, Ten Hoeve W, Carvelli M, Versteegen RM, Lub J, et al. Highly reactive trans-cyclooctene tags with improved stability for Diels-Alder chemistry in living systems. Bioconjugate Chem 2013;24:1210-7.

[15] Rossin R, van Duijnhoven SMJ, Läppchen T, van den Bosch SM, and Robillard MS. Trans-Cyclooctene Tag with Improved Properties for Tumor Pretargeting with the Diels-Alder Reaction. Mol Pharmaceutics 2014;11:3090-6.

[16] Zeglis BM, Brand C, Abdel-Atti D, Carnazza KE, Cook BE, Carlin S, et al. Optimization of a Pretargeted Strategy for the PET Imaging of Colorectal Carcinoma via the Modulation of Radioligand Pharmacokinetics. Mol Pharmaceutics 2015;12:3575-87.

[17] Meyer JP, Houghton JL, Kozlowski P, Abdel-Atti D, Reiner T, Pillarsetty NV, et al. (18)F-Based Pretargeted PET Imaging Based on Bioorthogonal Diels-Alder Click Chemistry. Bioconjugate Chem 2016;27:298-301.

[18] Houghton JL, Zeglis BM, Abdel-Atti D, Sawada R, Scholz WW, and Lewis JS. Pretargeted Immuno-PET of Pancreatic Cancer: Overcoming Circulating Antigen and Internalized Antibody to Reduce Radiation Doses. J Nucl Med 2016;57:453-9.

[19] Houghton JL, Membreno R, Abdel-Atti D, Cunanan KM, Carlin S, Scholz WW, et al. Establishment of the In Vivo Efficacy of Pretargeted Radioimmunotherapy Utilizing Inverse Electron Demand Diels-Alder Click Chemistry. Mol Cancer Ther 2017;16:124-33.

[20] Vugts DJ, Vervoort A, Stigter-van Walsum M, Visser GW, Robillard MS, Versteegen RM, et al. Synthesis of phosphine and antibody-azide probes for in vivo Staudinger ligation in a pretargeted imaging and therapy approach. Bioconjugate Chem 2011;22:2072-81.

[21] Neves AA, Stockmann H, Harmston RR, Pryor HJ, Alam IS, Ireland-Zecchini H, et al. Imaging sialylated tumor cell glycans in vivo. FASEB J 2011;25:2528-37.

[22] van den Bosch SM, Rossin R, Verkerk PR, ten Hoeve W, Janssen HM, Lub J, et al. Evaluation of strained alkynes for Cu-free click reaction in live mice. Nucl Med Biol 2013;40:415-23.

[23] Evans HL, Nguyen QD, Carroll LS, Kaliszczak M, Twyman FJ, Spivey AC, et al. A bioorthogonal (68)Ga-labelling strategy for rapid in vivo imaging. Chem Commun (Camb) 2014;50:9557-60.

[24] Denk C, Svatunek D, Filip T, Wanek T, Lumpi D, Frohlich J, et al. Development of a ^{18}F-labeled tetrazine with favorable pharmacokinetics for bioorthogonal PET imaging. Angew Chem Int Ed 2014;53:9655-9.

[25] Herth MM, Andersen VL, Lehel S, Madsen J, Knudsen GM, and Kristensen JL. Development of a (11)C-labeled tetrazine for rapid tetrazine-trans-cyclooctene ligation. Chem Commun (Camb) 2013;49:3805-7.

[26] Denk C, Svatunek D, Mairinger S, Stanek J, Filip T, Matscheko D, et al. Design, Synthesis, and Evaluation of a Low-Molecular-Weight (11)C-Labeled Tetrazine for Pretargeted PET Imaging Applying Bioorthogonal in Vivo Click Chemistry. Bioconjug Chem 2016;27:1707-12.

[27] Garcia MF, Zhang X, Shah M, Newton-Northup J, Cabral P, Cerecetto H, et al. (99m)Tc-bioorthogonal click chemistry reagent for in vivo pretargeted imaging. Bioorg Med Chem 2016;24:1209-15.

[28] Albu SA, Al-Karmi SA, Vito A, Dzandzi JP, Zlitni A, Beckford-Vera D, et al. (125)I-Tetrazines and Inverse-Electron-Demand Diels-Alder Chemistry: A Convenient Radioiodination Strategy for Biomolecule Labeling, Screening, and Biodistribution Studies. Bioconjug Chem 2016;27:207-16.

[29] Froidevaux S, Calame-Christe M, Tanner H, and Eberle AN. Melanoma targeting with DOTA-alpha-melanocyte-stimulating hormone analogs: structural parameters affecting tumor uptake and kidney uptake. J Nucl Med 2005;46:887-95.

[30] Akizawa H, Arano Y, Mifune M, Iwado A, Saito Y, Mukai T, et al. Effect of molecular charges on renal uptake of 111In-DTPA-conjugated peptides. Nucl Med Biol 2001;28:761-8.

[31] Keinänen O, Li XG, Chenna NK, Lumen D, Ott J, Molthoff CF, et al. A New Highly Reactive and Low Lipophilicity Fluorine-18 Labeled Tetrazine Derivative for Pretargeted PET Imaging. ACS Med Chem Lett 2016;7:62-6.

[32] Wijnen JW, Zavarise S, Engberts JBFN, and Charton M. Substituent Effects on an Inverse Electron Demand Hetero Diels−Alder Reaction in Aqueous Solution and Organic Solvents: Cycloaddition of Substituted Styrenes to Di(2-pyridyl)-1,2,4,5-tetrazine. J Org Chem 1996;61:2001-5.

[33] Maina T, Kaloudi A, Valverde IE, Mindt TL, and Nock BA. Amide-to-triazole switch vs. in vivo NEP-inhibition approaches to promote radiopeptide targeting of GRPR-positive tumors. Nucl Med Biol 2017;52:57-62.

[34] Ocak M, Helbok A, Rangger C, Peitl PK, Nock BA, Morelli G, et al. Comparison of biological stability and metabolism of CCK2 receptor targeting peptides, a collaborative project under COST BM0607. Eur J Nucl Med Mol Imaging 2011;38:1426-35.

[35] Linder KE, Metcalfe E, Arunachalam T, Chen J, Eaton SM, Feng W, et al. In vitro and in vivo metabolism of Lu-AMBA, a GRP-receptor binding compound, and the synthesis and characterization of its metabolites. Bioconjug Chem 2009;20:1171-8.

[36] Ocak M, Helbok A, von Guggenberg E, Ozsoy Y, Kabasakal L, Kremser L, et al. Influence of biological assay conditions on stability assessment of radiometal-labelled peptides exemplified using a 177Lu-DOTA-minigastrin derivative. Nucl Med Biol 2011;38:171-9.

[37] Valverde IE, Vomstein S, Fischer CA, Mascarin A, and Mindt TL. Probing the Backbone Function of Tumor Targeting Peptides by an Amide-to-Triazole Substitution Strategy. J Med Chem 2015;58:7475-84.

[38] Kaloudi A, Nock BA, Krenning EP, Maina T, and De Jong M. Radiolabeled gastrin/CCK analogs in tumor diagnosis: towards higher stability and improved tumor targeting. Q J Nucl Med Mol Imaging 2015;59:287-302.

Figure Legends

Fig. 1. Principle of tumor pretargeting with the inverse-electron-demand Diels–Alder (IEDDA) reaction between a *trans*-cyclooctene-tagged mAb and a radiolabeled tetrazine.

Fig. 2. Chemical structures of new tetrazine probes (**1a/b**, **2**, **3**), lead probe **4**, and schematic representation of clearing agent galactose-albumin-tetrazine (**5**) and *trans*-cyclooctene tagged CC49 (**6**).

Fig. 3. Synthetic strategy for preparation of new tetrazine probes **1a/b**, **2**, and **3**. Reagents and conditions: (A) $N_2H_4 \cdot H_2O$, S, EtOH, 70°C, o/n. Yields: **8a** - 66%, **8b** - 35%; (B) aq. $NaNO_2$, AcOH/THF. Yields: **9a** - 83%, **9b** - 75%; (C) TFA, $CHCl_3$, rt, 3 h; (D) DOTA-NHS, DIPEA, DMF, rt, 3 h. Yields over 2 steps: **1a** - 75%, **1b** - 79%; (E) BOP, DIPEA, DMF, rt, 2 h, 44%; (F) TFA, CH_2Cl_2, rt, o/n (2×), 69%; (G) TFA, CH_2Cl_2, rt, 2 h; (H) DIPEA, DMF, rt, 2 h, 27% over 2 steps.

Fig. 4. Blood clearance data of ^{177}Lu-labeled tetrazines (6.7 nmol, 0.6 – 1.0 MBq) in non-pretargeted tumor-bearing mice, fitted to a one-phase exponential decay model. Data points represent the % injected dose per gram (%ID/g) and are mean ± SD (n = 4). For calculated half-lives, see Table 1. The complete raw data is provided in Supplemental Table S6.

Fig. 5. Tumor-to-organ ratios from a biodistribution experiment of ^{177}Lu-labeled tetrazines (**1a**, **1b**, **2**, **3**, and **4**) in pretargeted LS174T tumor-bearing mice. The bar diagram is based on the experimental data reported in Table 2. Bars represent mean ± SD.

Table 1

Physicochemical properties, *in vitro* stability, reactivity and *in vivo* blood clearance of ^{177}Lu-labeled Tz-probes

Probe	MW [a] (g/mol)	$LogD_{7.4}$ mean ± SD	R_t (min) [b]	$t_{1/2}$ (h) PBS [c]	$t_{1/2}$ (h) 50% serum [d]	k_{obs} ($\times 10^{-2}$ s^{-1}) 50% serum [d][e]	$t_{1/2}$ (min) [f] Blood clearance
[^{177}Lu]**1a**	750.8	– 2.65 ± 0.01	9.7	27.3	11.3	10.0 ± 0.3	18.0
[^{177}Lu]**1b**	820.9	– 0.42 ± 0.02	12.7	19.0	0.8	13.1 ± 0.8	5.4
[^{177}Lu]**2**	793.8	– 3.27 ± 0.02	9.2	27.8	13.4	7.3 ± 0.3	17.5
[^{177}Lu]**3**	1443.6	– 4.25 ± 0.08	11.4	24.7	7.7	6.2 ± 0.4	11.3
[^{177}Lu]**4**	1278.4	– 4.51 ± 0.07	11.1	25.8	8.4	7.5 ± 0.5	10.7 [g]

[a] Molecular weight of the uncoordinated, metal-free probes. [b] RP-HPLC retention times.
[c] PBS pH 7.4, 37ºC. [d] 50% mouse serum / PBS, 37ºC. [e] Best-fit values (1st order exponential) ± standard error.
[f] For 95% confidence intervals and the complete raw data, see Supplemental Table S6.
[g] Taken from reference [13] (in mice bearing LS174T tumor xenografts pretargeted with CC49-TCO (**6**).

Table 2

Dual isotope biodistribution of [^{125}I]I-CC49-TCO (**6**) and ^{177}Lu-labeled tetrazines (**1a**, **1b**, **2**, **3**, and **4**) in pretargeted LS174T tumor-bearing mice. The mice were intravenously injected with [^{125}I]I-CC49-TCO (**6**) followed by 2 doses of clearing agent (**5**) after 30 h and 48 h, ^{177}Lu-labeled tetrazines (**1a**, **1b**, **2**, **3**, or **4**) after 50 h, and euthanasia/biodistribution after 53 h. Data are reported as mean ± SD (P-values refer to comparison with lead probe [^{177}Lu]**4**; * P < 0.01; ** P < 0.001). Uptake values for [^{125}I]ICC49-TCO (**6**) in the first column are combined data from pretargeting experiments with the new probes (**1a**, **1b**, **2**, and **3**), detailed data per group are reported in Supplemental Table S4. Data for [^{177}Lu]**4** were published previously [15].

Organ	^{125}I-CC49-TCO (**6**) *n = 13*	[^{177}Lu]**1a** *n = 4*	[^{177}Lu]**1b** *n = 3*	[^{177}Lu]**2** *n = 3*	[^{177}Lu]**3** *n = 3*	[^{177}Lu]**4** *n = 4*
	^{125}I (%ID/g)	**^{177}Lu (%ID/g)**	**^{177}Lu (%ID/g)**	**^{177}Lu (%ID/g)**	**^{177}Lu (%ID/g)**	**^{177}Lu (%ID/g)**
Tumor	20.71 ± 3.37	2.40 ± 0.90*	0.95 ± 0.41**	4.90 ± 0.62	2.72 ± 0.75*	6.13 ± 1.09
Blood	0.46 ± 0.18	0.11 ± 0.05	0.04 ± 0.01	0.09 ± 0.05	0.05 ± 0.02	0.03 ± 0.01
Heart	0.57 ± 0.14	0.07 ± 0.02	0.10 ± 0.03	0.06 ± 0.03	0.04 ± 0.01	0.04 ± 0.01
Lung	0.82 ± 0.18	0.40 ± 0.13	0.18 ± 0.06	0.38 ± 0.05*	0.25 ± 0.02	0.20 ± 0.06
Liver	1.88 ± 0.76	6.73 ± 1.40**	13.63 ± 1.06**	2.63 ± 0.30**	0.16 ± 0.02	0.18 ± 0.01
Spleen	0.70 ± 0.19	0.20 ± 0.05*	0.09 ± 0.06	0.11 ± 0.05	0.08 ± 0.02	0.09 ± 0.01
Kidney	0.49 ± 0.08	1.13 ± 0.16	0.27 ± 0.03**	1.27 ± 0.23	2.72 ± 0.27**	1.23 ± 0.19
Bladder	1.05 ± 0.29	0.41 ± 0.14	0.13 ± 0.05	1.10 ± 0.54	0.54 ± 0.08	0.54 ± 0.22
Muscle	0.25 ± 0.05	0.08 ± 0.04	0.14 ± 0.10	0.08 ± 0.06	0.07 ± 0.01*	0.02 ± 0.01
Bone	0.25 ± 0.06	0.09 ± 0.02	0.04 ± 0.00	0.07 ± 0.04	0.06 ± 0.01	0.05 ± 0.01
Brain	0.02 ± 0.01	0.01 ± 0.01	0.00 ± 0.00	0.01 ± 0.00	0.01 ± 0.00	0.01 ± 0.00
	%ID/organ	**%ID/organ**	**%ID/organ**	**%ID/organ**	**%ID/organ**	**%ID/organ**
Stomach	0.11 ± 0.03	0.06 ± 0.01*	0.08 ± 0.02*	0.07 ± 0.05	0.17 ± 0.05*	0.01 ± 0.01
Sm. intestine	0.47 ± 0.10	3.84 ± 1.55*	8.53 ± 1.20**	1.05 ± 0.23**	0.92 ± 0.35*	0.08 ± 0.02
Lg. intestine	0.51 ± 0.13	4.50 ± 1.01**	27.48 ± 2.79**	1.09 ± 0.24*	1.10 ± 0.07**	0.31 ± 0.12
Thyroid	0.60 ± 0.38	0.01 ± 0.00	0.01 ± 0.00	0.01 ± 0.00	0.01 ± 0.00	0.00 ± 0.00

Table 3

Biodistribution of ^{177}Lu-labeled tetrazines (**1a**, **1b**, **2**, and **3**) in non-pretargeted mice bearing LS174T colon carcinoma xenografts. The mice were intravenously injected with either [^{177}Lu]**1a**, [^{177}Lu]**1b**, [^{177}Lu]**2**, or [^{177}Lu]**3** and euthanized 3 h later. Data are reported as mean ± SD (P-values refer to comparison with the data of the same probe in pretargeted mice as provided in Table 2; * $P < 0.02$; ** $P < 0.002$).

Organ	[^{177}Lu]**1a** *n = 4*	[^{177}Lu]**1b** *n = 4*	[^{177}Lu]**2** *n = 4*	[^{177}Lu]**3** *n = 4*
	%ID/g	**%ID/g**	**%ID/g**	**%ID/g**
Tumor	0.64 ± 0.39*	0.06 ± 0.01*	0.55 ± 0.16**	0.38 ± 0.28**
Blood	0.11 ± 0.06	0.05 ± 0.01	0.08 ± 0.02	0.04 ± 0.01
Heart	0.08 ± 0.02	0.08 ± 0.01	0.07 ± 0.01	0.03 ± 0.00
Lung	0.60 ± 0.12	0.15 ± 0.01	0.52 ± 0.03*	0.19 ± 0.04
Liver	7.91 ± 1.93	12.44 ± 1.69	3.68 ± 0.40*	0.12 ± 0.01*
Spleen	0.25 ± 0.08	0.11 ± 0.03	0.17 ± 0.04	0.07 ± 0.01
Kidney	0.10 ± 0.04**	0.30 ± 0.02	2.04 ± 0.18*	2.04 ± 0.31
Bladder	1.72 ± 0.54*	0.14 ± 0.10	0.27 ± 0.04	0.31 ± 0.18
Muscle	0.29 ± 0.09*	0.04 ± 0.03	0.05 ± 0.01	0.03 ± 0.02
Bone	0.05 ± 0.01*	0.05 ± 0.02	0.10 ± 0.01	0.08 ± 0.06
Brain	0.09 ± 0.02**	0.02 ± 0.01	0.01 ± 0.00	0.01 ± 0.00
	%ID/organ	**%ID/organ**	**%ID/organ**	**%ID/organ**
Stomach	0.08 ± 0.06	0.10 ± 0.04	0.06 ± 0.02	0.04 ± 0.03*
Sm. intestine	4.67 ± 1.36	6.34 ± 2.23	1.61 ± 0.55	0.11 ± 0.01*
Lg. intestine	9.29 ± 1.35**	45.22 ± 3.16**	1.19 ± 0.53	0.96 ± 0.16

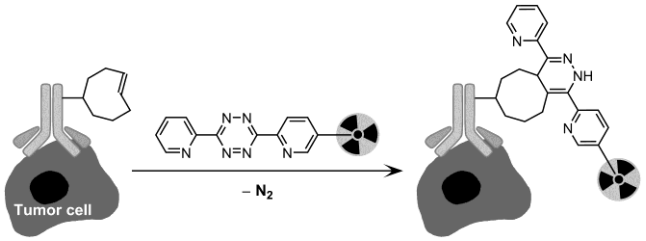

Fig. 1

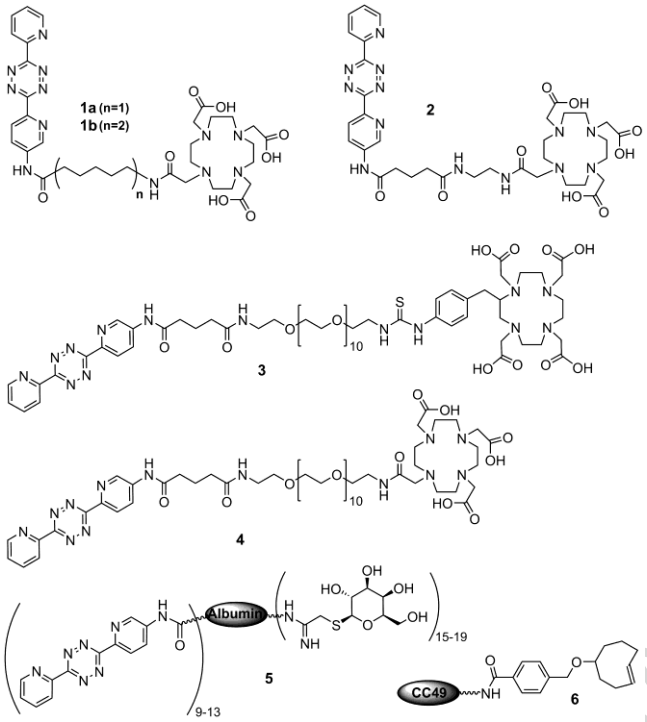

Fig. 2

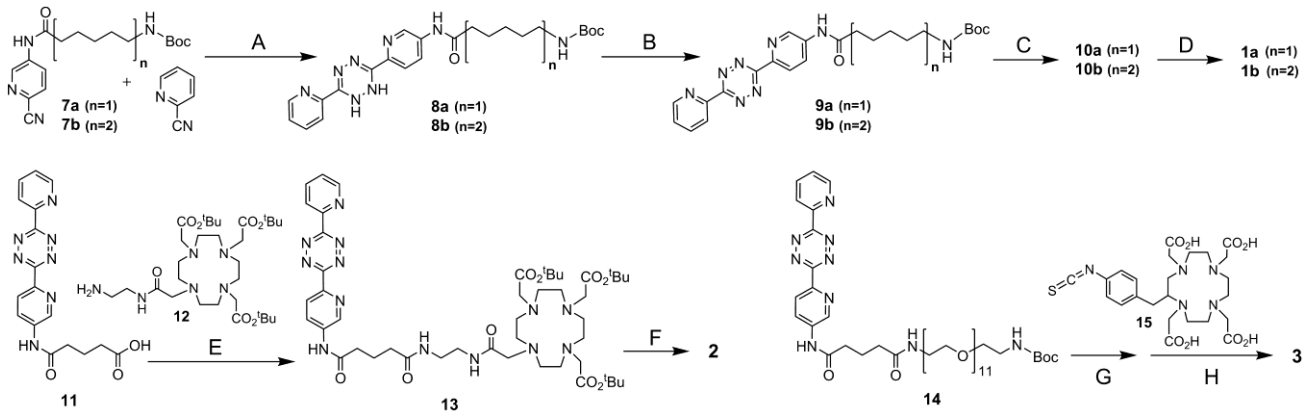

Fig. 3

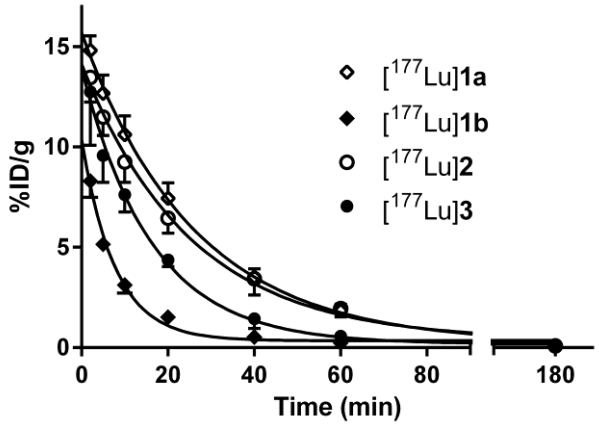

Fig. 4

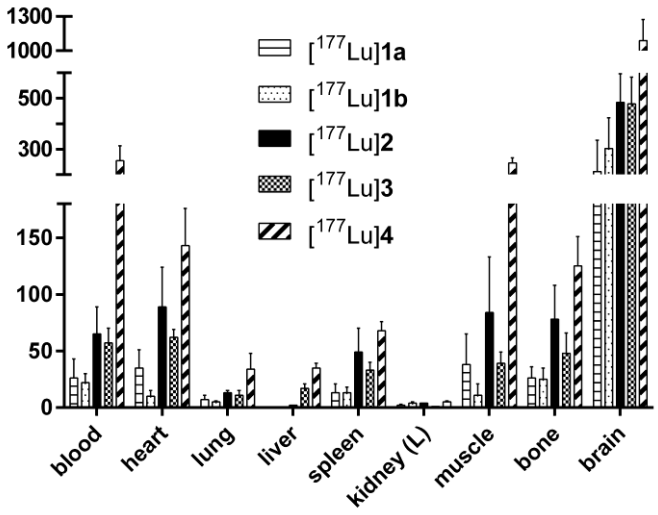

Fig. 5